(Received 3 December 2025, Accepted 12 February 2026, Scheduled 4 April 2026)

Dual-Band Textile C-Shape Complementary Split-Ring Metamaterial MIMO Antenna for Remote Health Monitoring

Hamza A. Mashagba[1], Hasliza A Rahim[2, 3, *], Nurul Anis Emillia Nazri[2], Mohd Najib Mohd Yasin[2, 3], Nur Hidayah Ramli[2, 3], Sarun Narongkul[4], Liyana Zahid[2, 3], Azlan B. Abd Aziz[1, *], and Samir Salem Al-Bawri[5]

[1] *Faculty of Engineering and Technology, Malaysia Centre for Wireless Technology (CWT) Multimedia University, 75450 Bukit Beruang, Melaka, Malaysia*
[2] *Faculty of Electronic Engineering & Technology, Universiti Malaysia Perlis, 02600 Arau Perlis, Malaysia*
[3] *Centre of Excellence for Advanced Communication Engineering (ACE) Universiti Malaysia Perlis, 01000 Kangar, Perlis, Malaysia*
[4] *Faculty of Industrial Technology, Songkhla Rajabhat University, Songkhla 90000, Thailand*
[5] *Space Science Centre, Institute of Climate Change, Universiti Kebangsaan Malaysia (UKM), 43600 Bangi, Selangor, Malaysia*

ABSTRACT: Background: Remote Health Monitoring Systems (RHMSs) rely on wearable antennas to enable the reliable wireless transmission of physiological data. However, existing wearable Multiple-Input Multiple-Output (MIMO) antennas often suffer from low gain and limited isolation, particularly under flexible and on-body conditions. **Methods:** This study proposes a dual-band textile C-shaped Complementary Split-Ring (CSR) Metamaterial (MTM)-based MIMO antenna operating at 2.45 GHz and 3.5 GHz. A metasurface layer composed of a 3×5 CSR array is integrated beneath the radiating elements to enhance isolation and realized gain. The antenna is evaluated under flat and bending conditions, and on-body performance is validated through Specific Absorption Rate (SAR) and Received Signal Strength Indicator (RSSI) measurements. **Results:** The proposed antenna achieves measured Mutual Coupling (MC) lower than -30 dB and realized gains of 2.45 dBi and 6.43 dBi at 2.45 GHz and 3.5 GHz, respectively. SAR values remain well below international safety limits, and RSSI measurements confirm improved communication performance over distances up to 10 m. **Conclusion:** The proposed dual-band textile metamaterial MIMO antenna provides a safe, flexible, and high-performance solution for wearable RHMS applications.

1. INTRODUCTION

RHMS enable continuous patient monitoring outside clinical environments using wearable and Internet of Things (IoT) devices [1]. The use of 5G wireless technology helps overcome the existing network's limitations with wider bandwidth, high data rates, low latency, and better quality of service [2]. In addition, there is an increased interest in less congested frequency bands, such as the 3.5 GHz mid-band of 5G technology [3], which is best suited for ensuring reliable RHMS [2]. Most of the traditional MC reduction techniques, such as Decoupling Network (DN) [4], hybrid defective ground structure (DGS), Frequency Selective Surfaces (FSS) [5], parasitic elements [6, 7], inter-element spacing along with reduced ground planes [8], and Electromagnetic Bandgap (EBG) structures [9], make the design more complex and/or less effective for flexible wearable technology platforms. In contrast, MTMs are artificially engineered structures that can effectively manipulate Electromagnetic (EM) wave propagation. Owing to these properties, MTMs have been widely employed in antenna design to enhance radiation characteristics, bandwidth, gain, and inter-element isolation [10].

Several MTM-based MIMO antennas have been reported in the literature. An Ultra-wideband (UWB) quad-port MIMO antenna employing MTM was presented, although it suffers from low gain [11]. A high-gain MTM-based MIMO antenna with excellent isolation was reported in [10]; however, it operates only in the 5G sub-6 GHz band and employs more than two MIMO elements. A textile metasurface-inspired MIMO antenna incorporating Reactive Impedance Surface (RIS) and EBG structures was proposed in [12], but it operates in a single band at 2.45 GHz with a low gain of 5.8 dBi. Similarly, wearable MTM-based MIMO antennas reported in [13] and [14] demonstrate good isolation and high gain but are limited to single-band operation in the 5–6 GHz range and involve more than two elements [14]. Other two-element MTM-based MIMO designs [15–17] achieve improved isolation; however, they either operate at higher frequencies and/or exhibit relatively low gain. Based on this analysis, none of the reported works simultaneously achieves dual-band operation, high gain, and flexibility using textile materials. To address this gap, this paper proposes a wearable dual-band textile MTM-based MIMO antenna for RHMS applications. The antenna operates at 2.45 GHz and 3.5 GHz, where the 2.45 GHz Industrial, Scientific, and Medical (ISM) band ensures global compatibility and reliable IoT connectivity, while the 3.5 GHz 5G mid-band

* Corresponding authors: Hasliza A Rahim (haslizarahim@unimap.edu.my); Azlan B. Abd Aziz (azlan.abdaziz@mmu.edu.my).

provides wider bandwidth and lower latency for real-time physiological data transmission. Together, these bands offer an optimal balance between communication range and system performance.

2. ANTENNA DESIGN

2.1. C-Shaped Complementary Split-Ring (CSR) MTM Unit Cell Design

A C-shaped CSR type of MTM unit cell is developed to control the electromagnetic response at the desired operating frequencies. The designed CSR unit cell acts as an LC circuit consisting of an inductor, L, and a capacitor, C. The conducting paths in the unit cell provide inductive behavior, whereas the small gaps between the paths provide capacitive coupling to confine the electric and magnetic fields. In the front view of the unit cell, as depicted in Fig. 1(a), the resonant path length and the gaps between the paths determine the operating frequencies. Fig. 1(b) shows the thickness of the MTM unit cell design. The layer structure in Fig. 1(c) emphasizes the placement of the conducting textile layer and textile substrate.

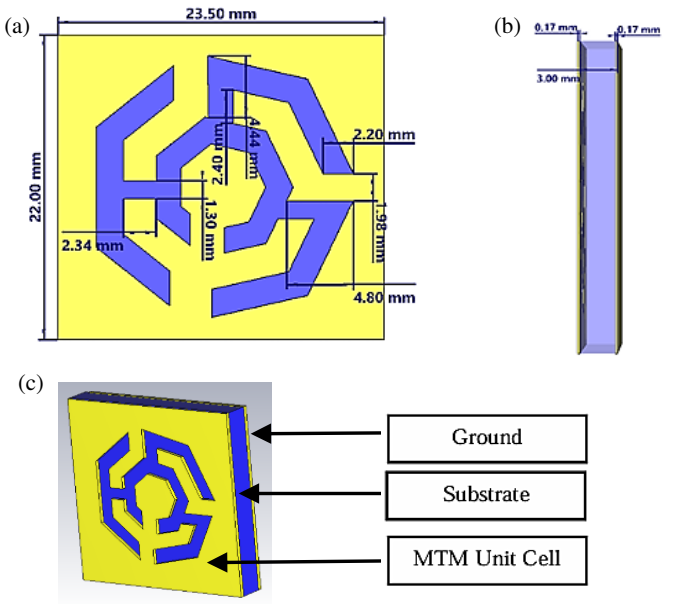

FIGURE 1. MTM unit cell design, (a) front view, (b) thickness, and (c) layers of the C-shaped CSR MTM.

The proposed MTM unit cell is simulated using Computer Simulation Technology (CST) Studio Suite with a time-domain solver over the 1–6 GHz frequency range. In the simulation setup, two waveguide ports are aligned along the positive and negative z-directions, with the unit cell positioned between them. Port 1 functions as the excitation (transmitting) port, while Port 2 serves as the receiving port to capture the transmitted response. A magnetic barrier is applied to the y-axis and an electric boundary to the x-axis. Furthermore, the Nicolson-Ross-Weir (NRW) technique is used to calculate effective parameters from simulated data [18]. The applicable equations are:

$$\varepsilon_r = \frac{2}{jk_0 d}\frac{1 - S_{21} + S_{11}}{1 + S_{21} - S_{11}} \tag{1}$$

$$\mu_r = \frac{j2S_{11}}{jk_0 d} + \mu_0 \tag{2}$$

$$n_r = \frac{2}{jk_0 d}\sqrt{\frac{(S_{21}-1)^2 - S_{11}^2}{(S_{21}+1)^2 - S_{11}^2}} \tag{3}$$

where S_{11} stands for the reflection coefficient, S_{21} for the transmission coefficient, ε_r for the permittivity, μ_r for the permeability, n for the refractive index, k_0 for the wave number, and d for the substrate thickness.

Figure 2 shows the effective parameters (ε_r and μ_r) of the MTM unit cell as a function of the frequency. The single C-shaped CSR exhibits a negative real part of permittivity and a positive real part of permeability in the 1–6 GHz range, indicating Single-Negative Permittivity (ENG) MTM behavior, as shown in Figs. 2(a)–(b). The negative slope of the permittivity confirms the ENG characteristic over the operating band. Meanwhile, the permeability demonstrates Mu-Near-Zero (MNZ) behavior near 2.45 GHz and 3.5 GHz, as shown in Fig. 2(b). Fig. 2(c) shows the positive refractive index values of the C-shaped CSR MTM unit cell. This combined ENG-MNZ response effectively redirects radiated energy toward the forward direction, enhances field confinement, and promotes constructive interference among MIMO elements, thereby making it possible to improve radiation efficiency and gain.

2.2. Dual-Band MIMO Antenna

The initial dual-band MIMO antenna is designed as in [6] to operate in dual-band mode, centered at 2.45 GHz for the lower band and 3.5 GHz for the upper band. The antenna has a total length of 70 mm and a width of 133.20 mm. A minor geometrical modification is introduced by increasing the inter-element spacing between the radiating patches from 0.1λ to 0.15λ, which slightly improves isolation performance, realized gain, and radiation efficiency. The perspective view with the locations of Ports 1 and 2 is shown in Fig. 3.

The substrate is Felt cloth, which is placed between the top radiator and the entire ground plane. The material has a relative permittivity (ε_r) of 1.44, a loss tangent ($\tan\delta$) of 0.044, and a thickness (H) of 3 mm [6]. ShieldIt Super electrotextile from LessEMF, Inc. is 0.17 mm thick and has an estimated conductivity of 1.18×10^5 Sm^{-1} [6]. In this work, antenna miniaturisation is not a design objective. Felt substrate is selected to maintain flexibility, conformability, and wearer comfort, while its low permittivity and low loss characteristics help maintain stable impedance matching and acceptable radiation performance, with priority given to wearability rather than size reduction.

2.3. Integration of C-Shaped CSR MTM into Dual-Band MIMO Antenna

The design evolution of the proposed MTM structure is performed in several stages to enhance isolation and realized gain

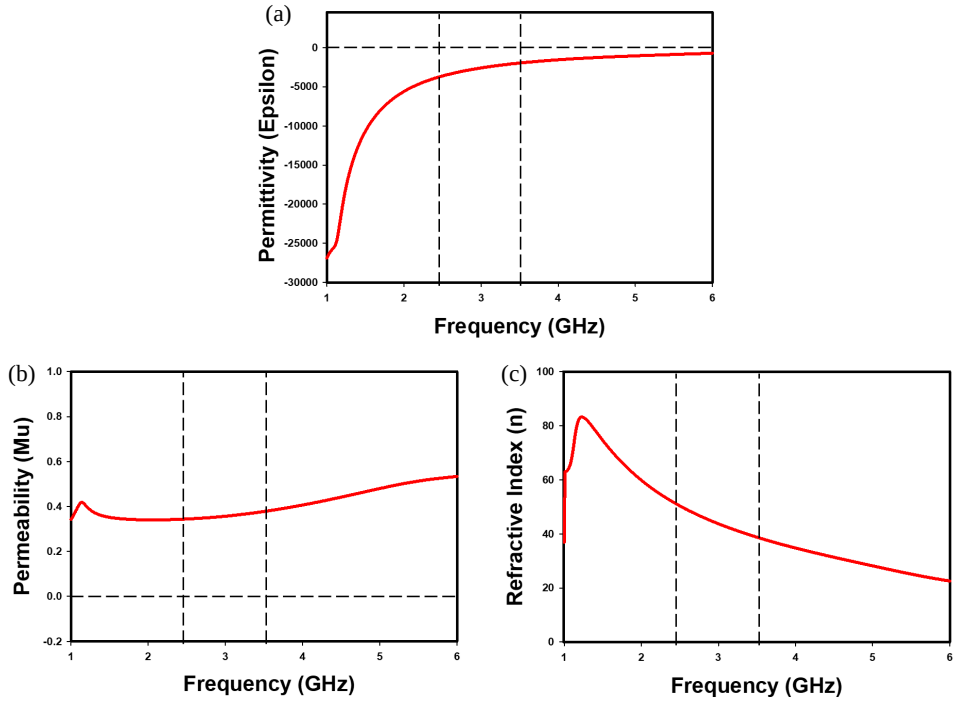

FIGURE 2. Simulated (a) permittivity, (b) permeability, and (c) refractive index of MTM unit cell.

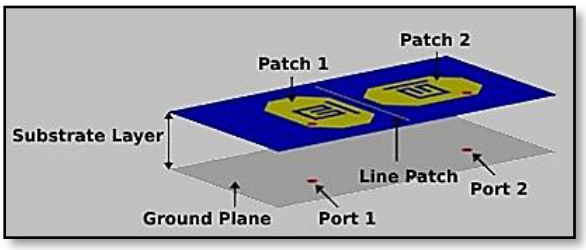

FIGURE 3. Perspective view of dual-band MIMO antenna [6].

of the dual-band MIMO antenna. Initially, a conventional dual-band MIMO antenna without MTM backing is developed; however, the strong surface currents and MC between the radiating elements limited the realized gain and radiation efficiency. To overcome these issues, a CSR-based unit cell is introduced. The first version uses a simple rectangular slot to confirm the ENG behavior, and the geometry is subsequently optimized into a C-shaped CSR configuration to provide stronger magnetic coupling and broader resonance bandwidth while maintaining compact size. The final stage integrated a 3×5 array of C-shaped CSR unit cells beneath the MIMO radiators, separated by a 20 mm air gap ($\varepsilon_r = 1$), forming a metasurface layer that suppresses surface waves and reduces MC between antenna ports. Fig. 4(a) provides a comprehensive view of the design and dimensions of the dual-band C-shaped CSR textile MIMO antenna; Fig. 4(b) shows the MTM array; and Fig. 4(c) shows the ground array. The antenna utilizes a 3×5 MTM etasurface with 1 mm inter-element spacing, matching the dimensions of the ground array.

The proposed antenna design consists of seven layers as presented in Fig. 4(a). The first layer is the top radiator or patch, which emits and receives signals. The second layer is a substrate made of Felt, providing a supportive base for the layers above. The third layer is the ground plane, which enhances the stability and performance of the antenna. The fourth layer is an air gap ($\varepsilon_r = 1$) to increase isolation between the antenna components. The fifth layer of the unit cell is organised in an array to maximise the channel capacity. The sixth and final layers are another substrate and ground array, providing stability and support to the unit cell. The optimization of the dual-band C-shaped CSR MTM MIMO antenna is performed based on the critical assessments of the radiator and C-shaped CSR unit cell, including slot length, ring width, separation, and periodicity, to achieve a dual-band response at 2.45 GHz and 3.5 GHz.

2.4. Dual-Band C-Shaped CSR MTM MIMO Antenna Integrated with RHMS

A MAX30102 sensor and an LM35 module are placed on the patient's finger to measure the body temperature, oxygen saturation (SpO_2), and heart rate. These sensors and the proposed antenna are integrated into the ESP32. This proposed MIMO antenna enhances the transmission medium for transmitting and receiving data at varied distances. The distance between the hardware with integrating the proposed antenna and the mobile application (MIT App Inventor) will be varied from 1 m to 10 m based on RSSI. Then, all the collected data are transmitted to the MIMO antenna via a Wi-Fi module. Lastly, the data are sent to the mobile application through the phone. Healthcare personnel can access these data periodically, allowing them to monitor the patient's vital signs over time. To experimentally validate the simulated performance, the fabricated prototype of the dual-band C-shaped CSR textile MIMO antenna is characterized using a Vector Network Analyzer (VNA, Keysight E5071C). The measurements are conducted at Universiti Malaysia Perlis'

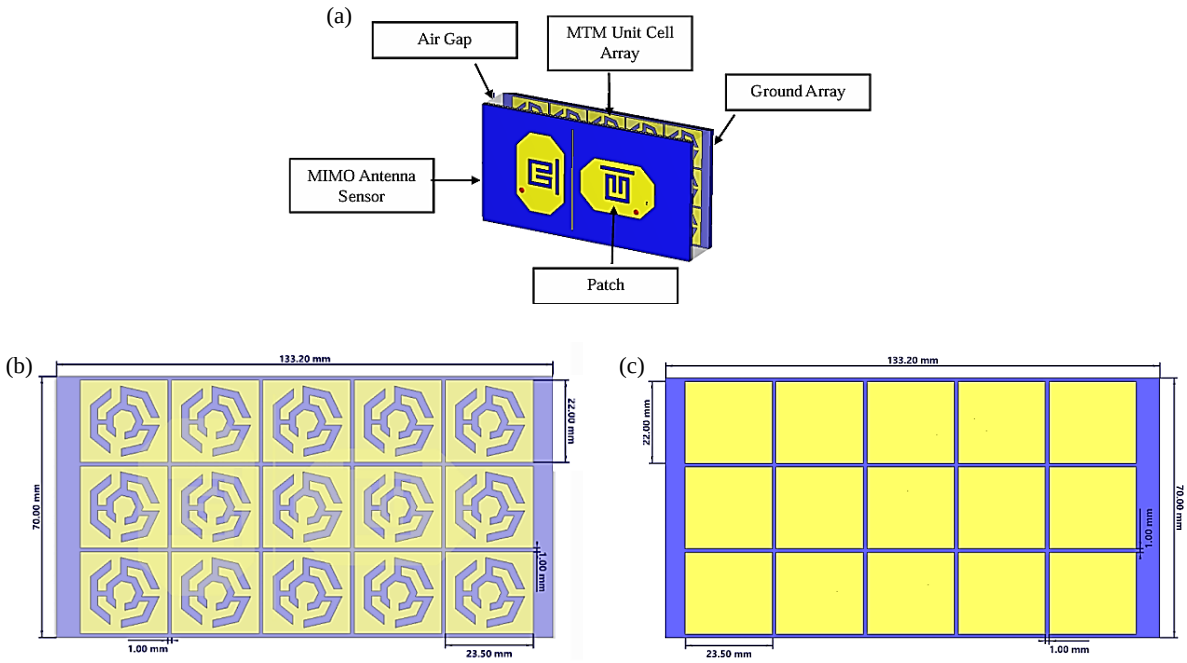

FIGURE 4. (a) Perspective view, (b) dimension of MTM array, and (c) dimension of ground array of the dual-band C-shaped CSR MTM textile MIMO antenna sensor.

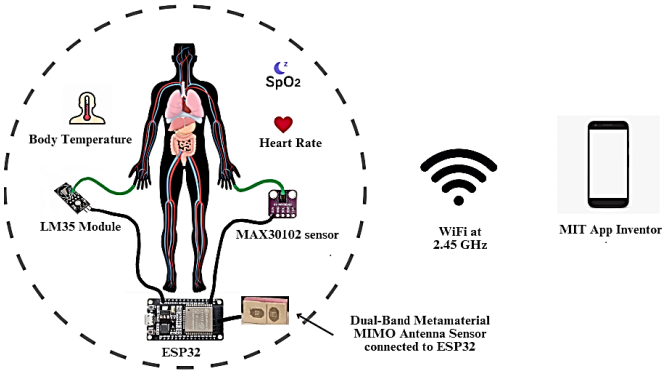

FIGURE 5. Experimental setup for the proposed MIMO antenna with RHMS.

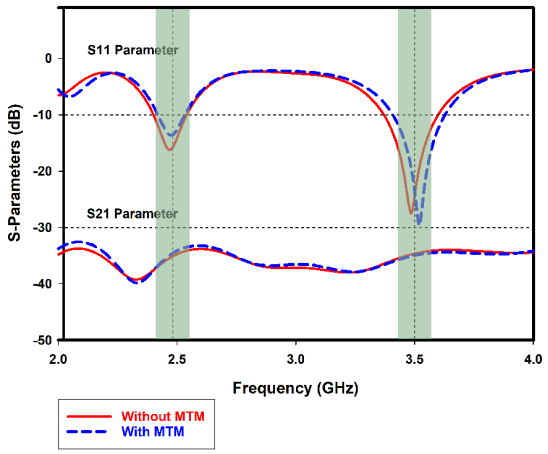

FIGURE 6. S-parameters of the proposed MIMO antenna with and without MTM.

Center of Excellence for Advanced Communication Engineering (ACE) (UniMAP). The antenna is connected via flexible SMA connectors, and each port is individually matched and calibrated. The prototype is tested under two conditions: on-body (arm & chest) and free-space placements. Fig. 5 shows the laboratory measurement setup, where the antenna is mounted on a low permittivity foam block to emulate the human-body curvature while maintaining a consistent distance from the ground plane. The same setup is later used for on-body tests, where the antenna is attached to a cotton layer placed on the human arm and chest to ensure safe exposure during measurements.

3. RESULTS AND DISCUSSION

3.1. S-Parameters, Realized Gain and Radiation Efficiency

Figure 6 shows the S_{11} and S_{21} characteristics of the proposed MIMO antenna. The antenna exhibits reflection coefficient values of more than -20 dB and less than -25 dB at 2.45 GHz and 3.5 GHz, respectively, with and without MTM. The MC (S_{21}) is consistent below -30 dB, with or without MTM integration for both bands. Besides, Fig. 7 presents the realized gain comparison with and without MTM. The MTM-integrated design increases the realized gain from 1.87 dBi to 2.45 dBi (+31.4%) at 2.45 GHz and from 5.8 dBi to 6.43 dBi (+10.9%) at 3.5 GHz. In this design, the MTM array functions as a reflector, effectively suppressing backward radiation and manipulating the EM waves to radiate in phase, thereby enhancing radiation efficiency and improving antenna gain [10]. Figs. 8(a)–(b) show the radiation-efficiency results. Without the MTM, efficiencies of 24% at 2.45 GHz and 48% at 3.5 GHz are obtained. With the integration of the C-shaped CSR array, these values increase slightly to 27% and 52%, respectively, indicating a

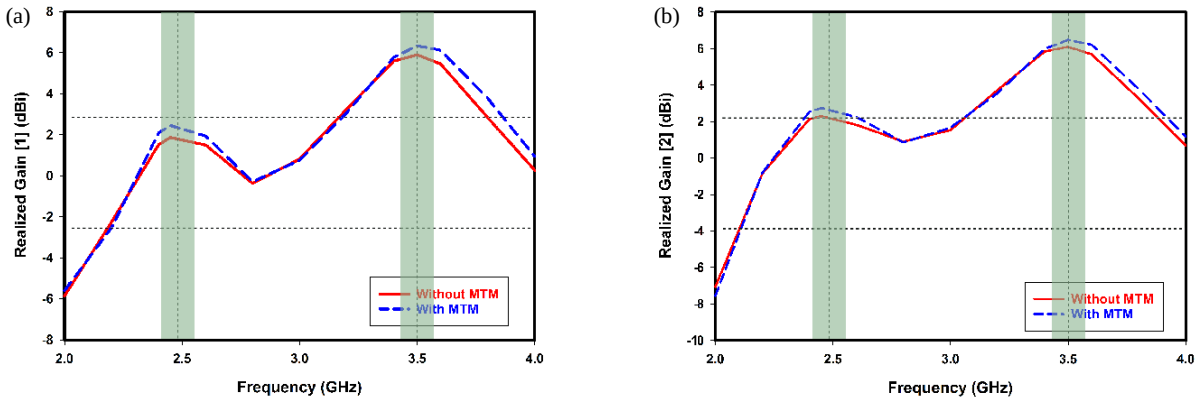

FIGURE 7. Realized gains of the proposed MIMO antenna with and without MTM unit cell array at (a) Port 1 and (b) Port 2.

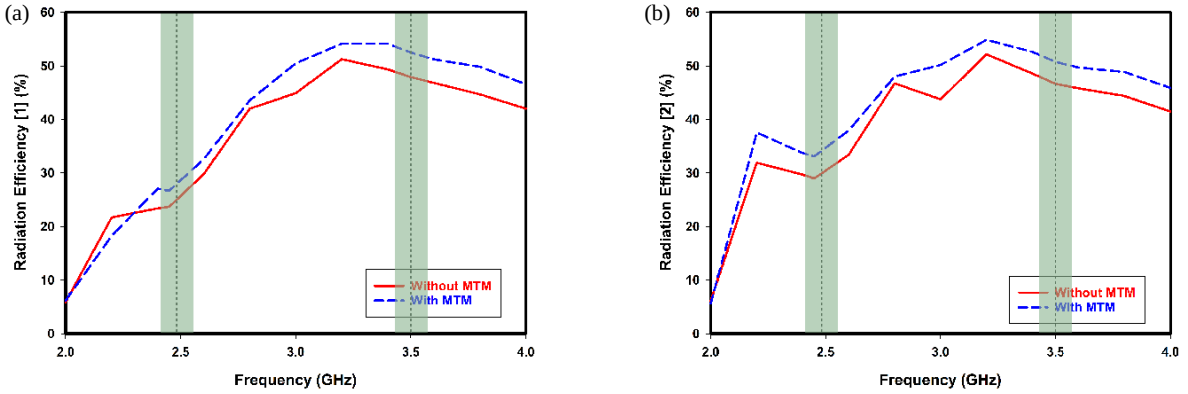

FIGURE 8. Radiation efficiencies of the proposed MIMO antenna with and without MTM unit cell array at (a) Port 1 and (b) Port 2.

clear improvement in radiating capability. Although the enhancement in gain is substantial, the improvement in radiation efficiency is limited due to inherent limitations in wearable antennas, such as Felt substrate loss, ohmic loss in flexible wires, and EM absorption due to human body proximity. Although MTM improves the confinement of the electric field and radiation directivity, thus enhancing gain, it does not overcome these loss limitations. Nevertheless, the results confirm that MTM integration positively influences both impedance characteristics and radiation performance, despite the need for further gain optimization. Table 1 compares the antenna's realized gains and radiation efficiencies with and without MTM integration.

3.2. Radiation Pattern

Figure 9 depicts the intended MIMO antenna radiation patterns for both ports and operating frequencies. Figs. 9(a) and 9(c) show radiation patterns at 2.45 GHz for Ports 1 and 2, respectively, while Figs. 9(b) and (d) are radiation patterns at 3.5 GHz. The results verify a directive pattern in all configurations, a proof of the antenna's capability for directed signal transmission in RHMS.

3.3. Bending Evaluation

Figure 10 illustrates various bending configurations that are introduced to the proposed MIMO antenna. The efficiency of the

TABLE 1. Summary of the comparison performance of the antenna's realized gain and radiation efficiency with and without MTM integration.

Parameter	f (GHz)	Without MTM	With MTM	Improvement
Realized gain (dBi)	2.45	1.87	2.45	+31.4%
Realized gain (dBi)	3.5	5.8	6.43	+10.9%
Radiation efficiency (%)	2.45	24	27	+12.5%
Radiation efficiency (%)	3.5	48	52	+8.3%

bent antenna configurations is assessed against the simulated flat condition, as shown in Fig. 11. As the bending angle increases from 45° to 60° along x- & y-axes, the proposed MIMO antenna experiences noticeable impedance mismatch, observed as a downward shift in the resonant frequencies in both operating bands. This behavior is attributed to changes in the effective electrical length and current distribution caused by mechanical deformation, and the impact was more pronounced in the top band. When the antenna is bent along the x-axis, a slight drop in S_{21} occurs. With increasing bending angle at 2.45 GHz, in-

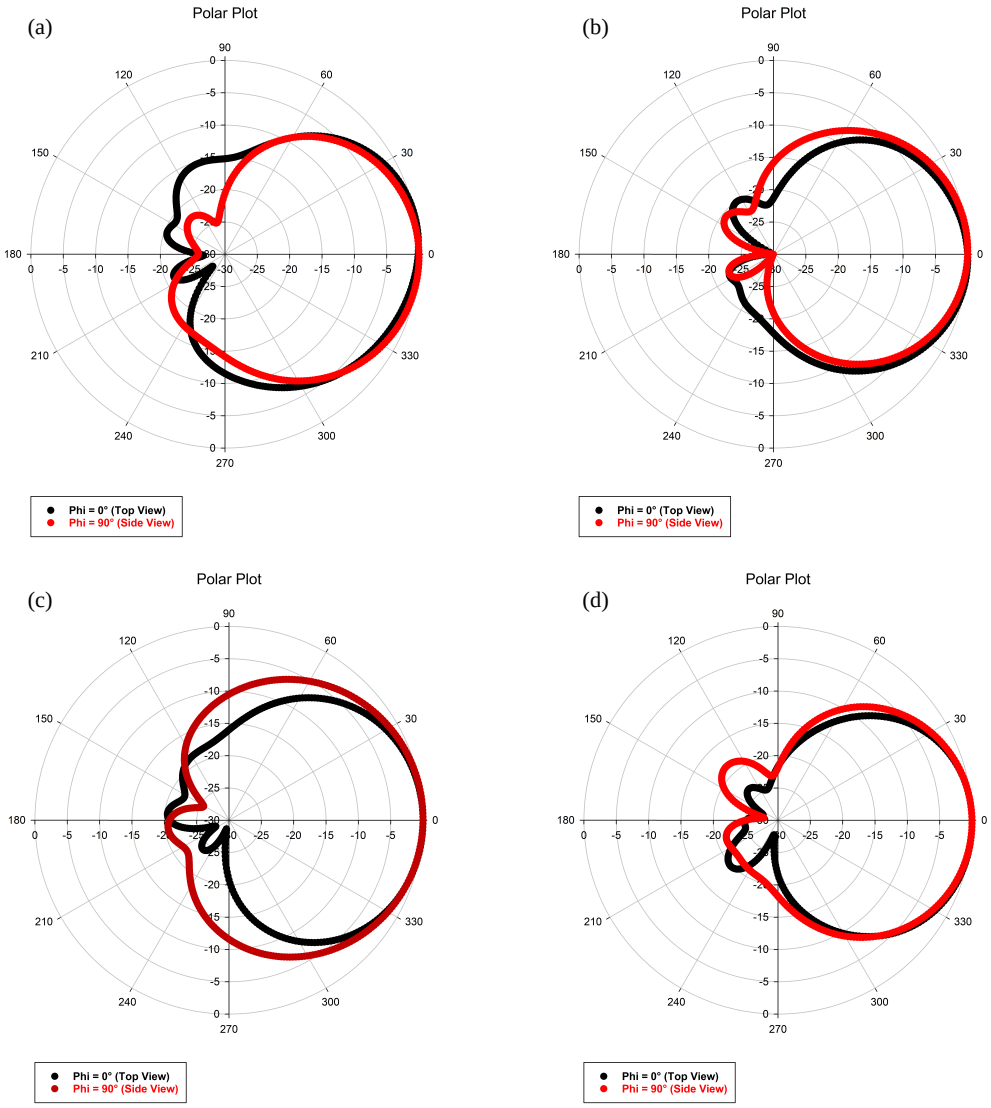

FIGURE 9. Radiation patterns of the proposed MIMO antenna, (a) 2.45 GHz at Port 1, (b) 3.5 GHz at Port 1, (c) 2.45 GHz at Port 2, and (d) 3.5 GHz at Port 2.

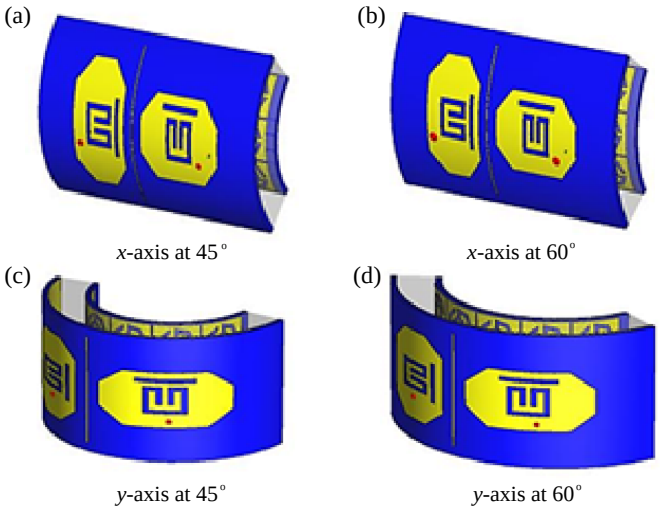

x-axis at 45° *x*-axis at 60°

y-axis at 45° *y*-axis at 60°

FIGURE 10. Various bending configurations of the proposed MMO antenna.

dicating lower MC, a similar trend is also observed at 3.5 GHz. In contrast, bending along the y-axis results in fluctuations of S_{21} in the lower frequency band, while the upper band remains relatively stable. As expected, bending at 60° yields the MC < -30 dB at both operating frequencies. Overall, these results indicate that antenna bending at different angles causes only minor variations in MC, demonstrating stable isolation performance across both frequency bands.

The bending along the x-axis at an angle of 60° ensures the maintenance of positive gain for both operating frequencies for the two ports, indicating no degradation and the possibility of improvement in the efficiency of signal transmission, as depicted in Figs. 12(a)–(b). On the other hand, y-axis bending at 45° and 60° has a significant impact on the reduction of gain, especially for Port 2 at 3.5 GHz, which indicates the sensitivity of the antenna to y-axis deformation, especially at higher frequency. Figs. 13(a) shows an increase in radiation efficiency for Port 1 in the lower band, while a significant decrease in ra-

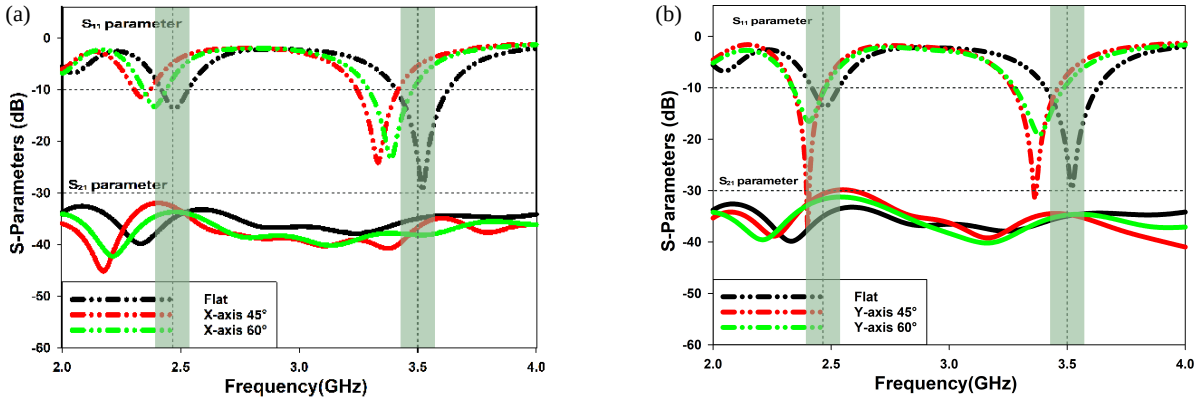

FIGURE 11. S-parameters of the proposed MIMO antenna at (a) x-axis and (b) y-axis.

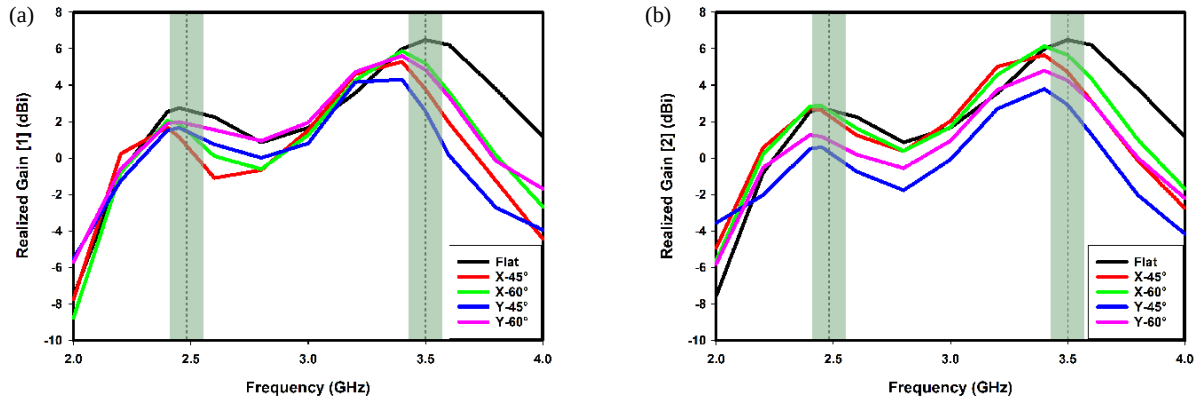

FIGURE 12. Realized gains of the proposed MIMO antenna for various bends at (a) Port 1 and (b) Port 2.

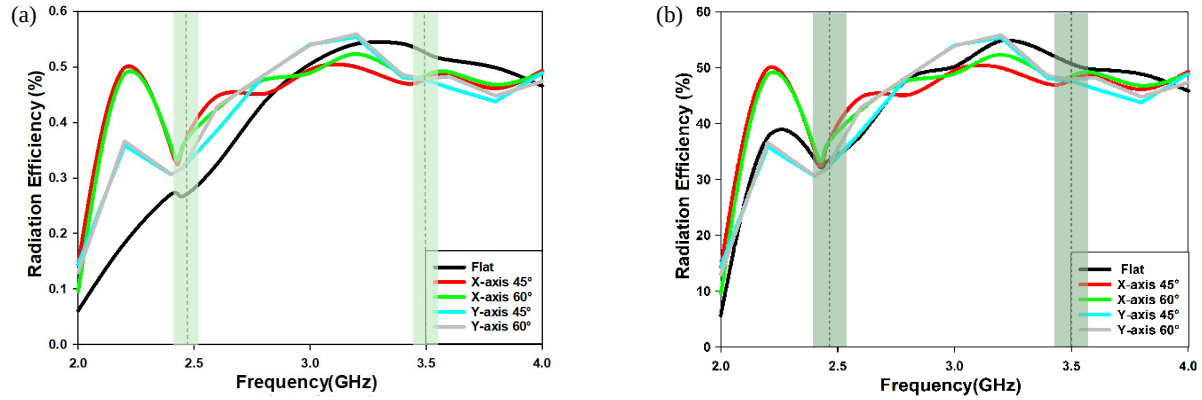

FIGURE 13. Radiation efficiencies of the proposed MIMO antenna for various bends at (a) Port 1 and (b) Port 2.

diation efficiency is observed in the upper band under all bending conditions. Fig. 13(b) indicates that the antenna maintains the radiation efficiency for Port 2 after 45° bending along the x-axis, whereas the efficiency decreases in the upper band with 60° bending along both the x-axis and y-axis. With 45° y-axis bending, moderate efficiency is maintained, with a minor reduction in efficiency in the lower frequency and a more significant reduction in the efficiency for Port 2 at 3.5 GHz.

In terms of the radiation characteristics, the main lobe is maintained under all the bending conditions, whereas an increase in the back lobe level is observed with the reduction of the bending angle from 60° to 45° in both the bending directions, as depicted in Fig. 14. More significant changes in the antenna pattern occur when the y-axis bending causes the primary lobe to lean to the right at $\varphi = 0°$ in both the lower and higher bands (Figs. 14(a) and (c)). In the upper band, the antenna pattern becomes somewhat wider than the flat conditions with moderately higher back lobe levels. Nevertheless, the proposed MIMO antenna consistently maintains a forward-directed radiation pattern across all bending scenarios. This confirms that the antenna preserves its directional radiation characteristics under mechanical deformation, which is essential for reliable

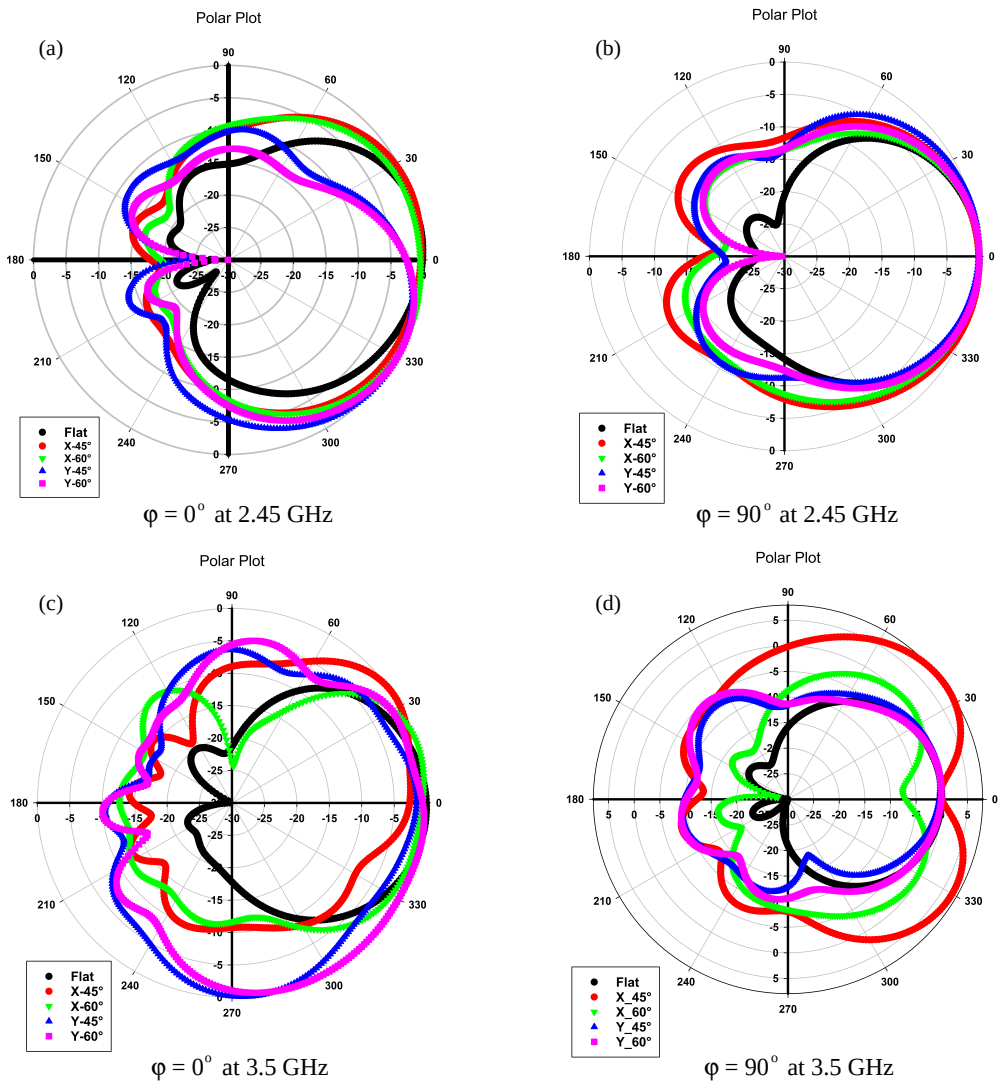

FIGURE 14. Radiation patterns of the proposed MIMO antenna under bending, (a) $\varphi = 0^\circ$ at 2.45 GHz, (b) $\varphi = 90^\circ$ at 2.45 GHz, (c) $\varphi = 0^\circ$ at 3.5 GHz and (d) $\varphi = 90^\circ$ at 3.5 GHz.

on/off-body communication, reduced body absorption, and stable data transmission in wearable RHMS applications.

3.4. Specific Absorption Rate (SAR) Evaluation

The SAR evaluations are conducted at various body locations within the CST Hugo voxel model, including the arm, chest, and back regions, to account for variations in tissue composition, thickness, and antenna placement. In accordance with the guidelines established according to the International Commission on Non-Ionizing Radiation Protection (ICNIRP) and the IEEE C95.1-2019 standard, the average SAR for on-body applications cannot exceed 1.6 W/kg averaged over 1 g of tissue or 2.0 W/kg averaged over 10 g of tissue [5]. In this work, SAR analysis is carried out by mounting the suggested MTM MIMO antenna on the Right Upper Arm (RUA) at operating frequencies of 2.45 GHz and 3.5 GHz (Fig. 15). For the 1 g tissue averaging case, as illustrated in Fig. 16(a) and Fig. 17(a), the SAR distributions exhibit localized regions of elevated radio frequency (RF) energy absorption concentrated around the antenna elements, as indicated by the red and yellow regions.

Owing to the smaller averaging mass, the absorbed RF energy is more localized, resulting in higher peak SAR values. For the 10 g tissue mass, the SAR distributions shown in Fig. 16(b) at 2.45 GHz and Fig. 17(b) at 3.5 GHz exhibit a more diffused pattern, where RF energy is distributed over a larger tissue volume, thereby reducing localized heating effects. Fig. 18 illustrates the placement of the proposed MTM MIMO antenna on the Right Chest (RC) and the corresponding on-body radiation patterns at 2.45 GHz and 3.5 GHz. The radiation analysis considers excitations at both Port 1 and Port 2, indicating the EM wave propagation behavior when the antenna operates in close proximity to the human torso. The presence of the lossy chest tissues significantly influences the radiation characteristics, resulting in pattern distortion compared to free-space operation and a dominant radiation directed away from the body. The SAR distributions for the RC and right back (RB) configurations are presented in Figs. 19 and 20, respectively. In particu-

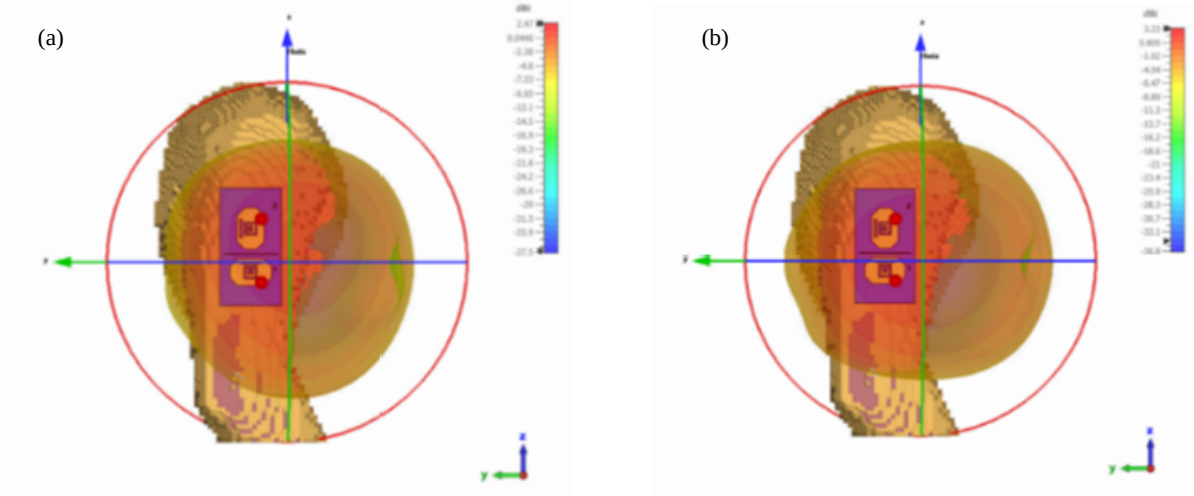

FIGURE 15. The radiation pattern of the MTM MIMO antenna on RUA for (a) 2.45 GHz and (b) 3.5 GHz.

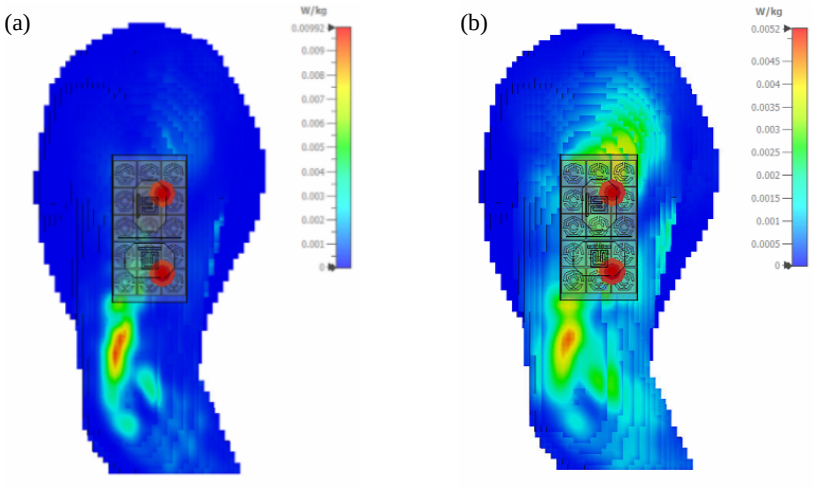

FIGURE 16. Peak SAR values for (a) 1 g and (b) 10 g of tissue at Port 1 placed on RUA at the frequency of 2.45 GHz. (a) SAR_{Max} = 0.0103. (b) SAR_{Max} = 0.0054.

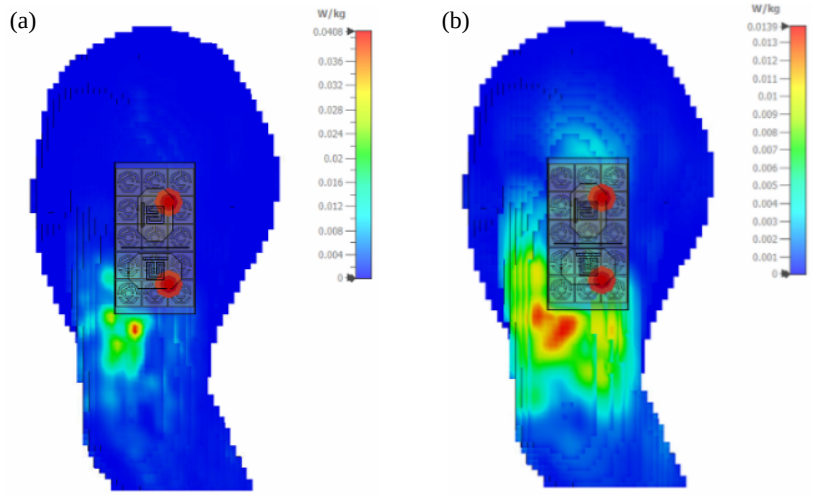

FIGURE 17. Peak SAR values for (a) 1 g and (b) 10 g of tissue at Port 1 at frequency of 3.5 GHz. (a) SAR_{Max} = 0.0479. (b) SAR_{Max} = 0.0142.

lar, the SAR distributions on the RB with Port 1 excitation are shown in Fig. 19 and Fig. 20 for 2.45 GHz and 3.5 GHz, respectively, evaluated over both 1 g and 10 g of tissue.

For the 10 g tissue averaging case, the SAR distributions are more spatially dispersed, indicating reduced localized RF energy concentration and lower thermal impact. The maximum SAR values recorded are 0.0150 W/kg at 2.45 GHz and

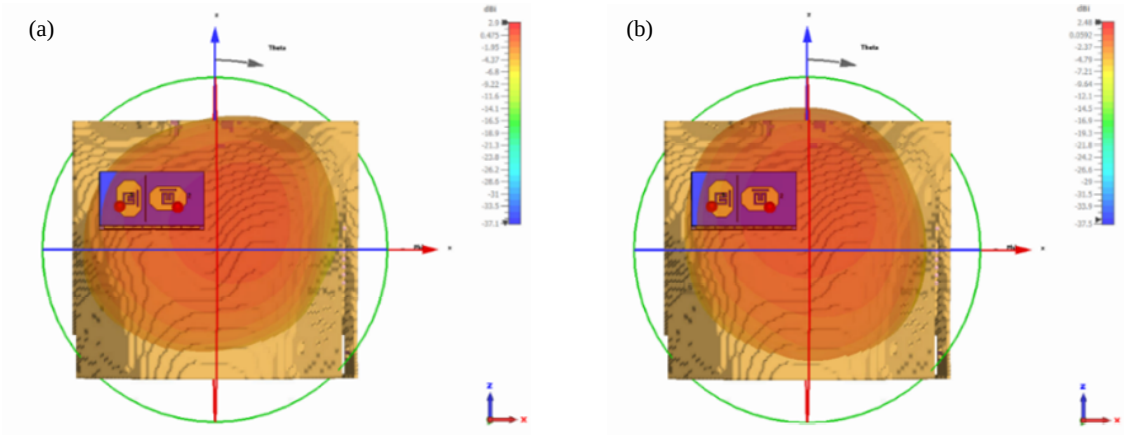

FIGURE 18. The radiation patterns of the MTM MIMO antenna on RC for (a) 2.45 GHz and (b) 3.5 GHz.

TABLE 2. SAR values of 1 g at different distances between MTM MIMO antenna and on-body regions.

	2.45 GHz		3.5 GHz	
	Port 1	Port 2	Port 1	Port 2
Distance (mm)	RUA			
0	0.0103	0.0119	0.0479	0.0422
5	0.0240	0.0117	0.0456	0.0401
10	0.0270	0.0125	0.0387	0.0373
	RC			
0	0.0169	0.0121	0.0189	0.0359
5	0.0197	0.0097	0.0197	0.0355
10	0.0123	0.0071	0.0150	0.0296
	RB			
0	0.0232	0.0193	0.0328	0.0479
5	0.0201	0.0152	0.0282	0.0333
10	0.0173	0.0124	0.0343	0.0282

TABLE 3. SAR values of 10 g at different distances between MTM MIMO antenna and on-body regions.

	2.45 GHz		3.5 GHz	
	Port 1	Port 2	Port 1	Port 2
Distance (mm)	RUA			
0	0.0054	0.0069	0.0142	0.0126
5	0.0109	0.0054	0.0160	0.0118
10	0.0116	0.0055	0.0149	0.0107
	RC			
0	0.0110	0.0066	0.0090	0.0165
5	0.0089	0.0052	0.0073	0.0111
10	0.0075	0.0046	0.0050	0.0073
	RB			
0	0.0150	0.0112	0.0143	0.0178
5	0.0120	0.0091	0.0121	0.0146
10	0.0099	0.0074	0.0135	0.0120

0.0143 W/kg at 3.5 GHz. Variations in SAR values across different body locations are mainly influenced by tissue composition and antenna placement. Regions such as the chest exhibit slightly higher SAR than the arm, as in [5]. Moreover, the antenna's broadside radiation pattern directs EM energy away from the body. All SAR levels remain well below the limits specified by international safety limits, verifying that the suggested MTM MIMO antenna is suitable for on-body RHMS applications.

3.5. Effect of Distance Between MTM MIMO Antenna and the Human Model on SAR Distribution

Tables 2 and 3 summarize the SAR values averaged over 1 g and 10 g of tissue at antenna-to-body separation distances of 0 mm, 5 mm, and 10 mm for both lower and upper operating bands. The results show that most of the SAR values are the highest when the antenna makes direct contact with the body (0 mm) and decrease progressively as the separation increases to 5 mm and 10 mm. This trend is consistent for both 1 g and 10 g evaluations. At 0 mm separation, the highest SAR for the 1 g evaluation is 0.0479 W/kg at 3.5 GHz (RUA, Port 1), while for 10 g, the highest value is 0.0178 W/kg at 3.5 GHz (RB, Port 2). Increasing the antenna-to-body distance to 5 mm results in a notable SAR reduction of approximately 10–20% across all body locations and frequencies. This behavior is attributed to strong near-field coupling once the antenna is near the body, which diminishes with increasing separation. In some cases, minor SAR fluctuations at intermediate distances may occur due to impedance matching variations and near-field interactions with multilayer tissue structures; however, SAR consistently decreases at larger separations.

3.6. MIMO Diversity Analysis

3.6.1. Envelope Correlation Coefficient (ECC)

Envelope Correlation Coefficient (ECC) is used to assess the degree of correlation among antenna [19] components. Lower ECC values imply higher isolation between antennas, ensuring that signals broadcast and received are uncorrelated, which enhances diversity performance and improves overall system capacity. For an efficient MIMO system, ECC should be less

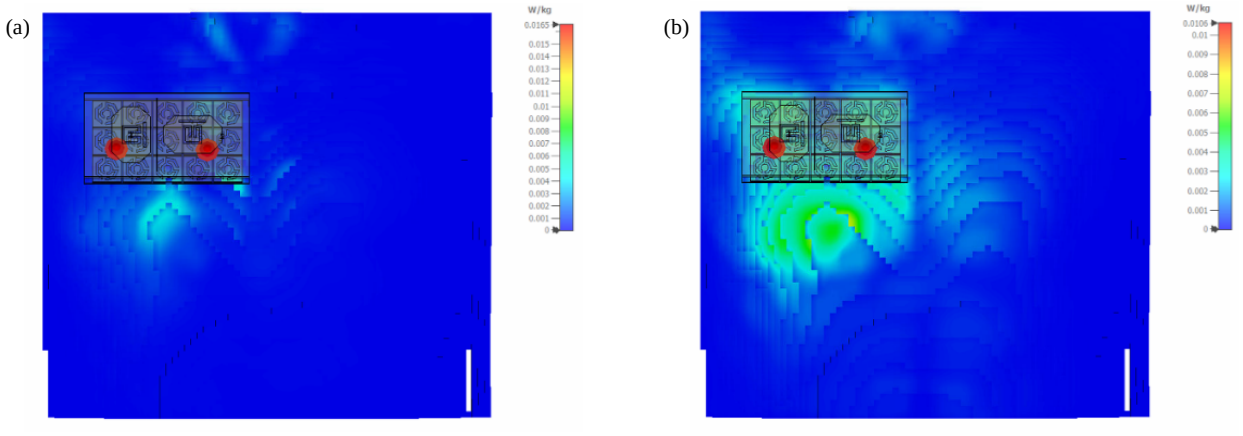

FIGURE 19. The RC's SAR distribution at Port 1 for (a) 1 g and (b) 10 g of tissue for 2.45 GHz. (a) SAR_{Max} = 0.0169. (b) SAR_{Max} = 0.0110.

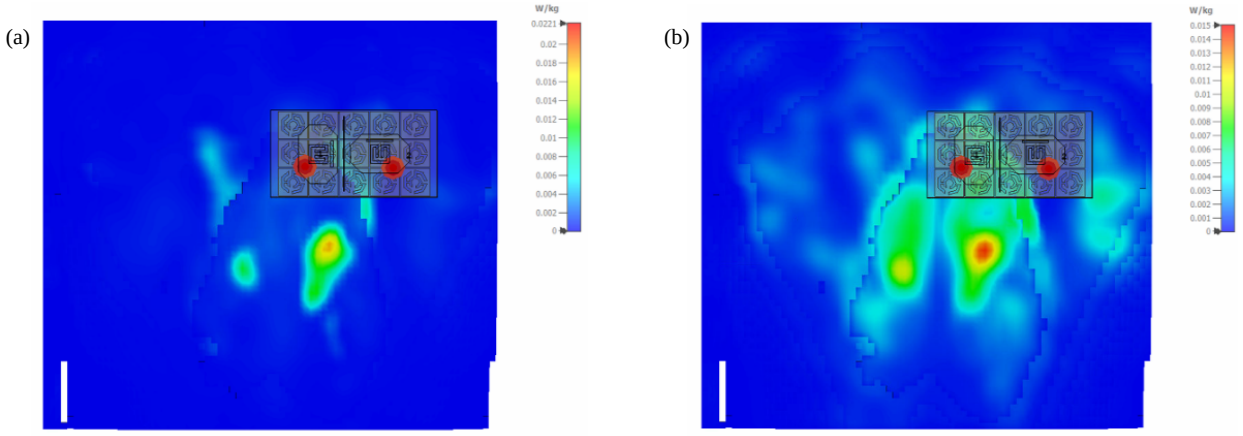

FIGURE 20. The RB's SAR distribution at Port 1 for (a) 1 g and (b) 10 g of tissue for 3.5 GHz. (a) SAR_{Max} = 0.0233. (b) SAR_{Max} = 0.0150.

than 0.3, ideally approaching zero. The MIMO diversity analysis of the proposed MTM MIMO antenna is conducted using the Spyder application in an Integrated Development Environment (IDE) for Python, within the Anaconda environment. The ECC, based on the total far-field electric fields, can be expressed as:

$$\rho_e = \frac{\left| \iint \left[\vec{E}_1(\theta,\varphi) \cdot \vec{E}_2^*(\theta,\varphi) \right] d\Omega \right|^2}{\iint \left| \vec{E}_1(\theta,\varphi) \right|^2 d\Omega \iint \left| \vec{E}_2(\theta,\varphi) \right|^2 d\Omega}$$

where $\vec{E}_1(\theta,\varphi)$ and $\vec{E}_2(\theta,\varphi)$ represent the total far-field electric fields of Antenna 1 and Antenna 2. θ, φ and E^* are the elevation angle, azimuth angle, and complex conjugate of the electric field. From the equation, the differential solid angle element $d\Omega$ is defined as:

$$d\Omega = \sin\theta d\theta d\varphi$$

with $\theta = (0 \text{ to } \pi)$ and $\varphi = (0 \text{ to } 2\pi)$. Fig. 21 shows that ECC calculated from radiation patterns without phase information yields higher values, reaching up to 0.5 at 2 GHz, indicating that neglecting spatial correlation and antenna directivity leads to overestimation. By incorporating polarization and phase information, Fig. 21 demonstrates a significant reduction in ECC, with values consistently below 0.035, providing a more accurate assessment of antenna correlation. Overall, the ECC results in Figs. 21 and 22 remain well below the 0.3 threshold, confirming excellent isolation and the suitability of the proposed metamaterial MIMO antenna for optimal MIMO performance.

3.6.2. Diversity Gain (DG) and Channel Capacity Loss (CCL)

Diversity Gain (DG) is an important performance metric in MIMO antenna systems that measures the improvement in signal reception gained by diversity approaches [20]. It evaluates the antenna system's ability to counteract multipath fading by capturing multiple independent signal paths. DG is calculated using the ECC as:

$$DG = 10 \times \sqrt{1 - ECC^2}$$

ECC assesses the relationship between the radiation patterns of MIMO antenna elements. Fig. 22 shows that the DG derived from radiation-pattern-based ECC remains close to 10 dB across 2 to 4 GHz, indicating strong diversity performance, enhanced signal reception, minimal signal correlation, and the effective mitigation of multipath fading for the proposed MTM MIMO antenna.

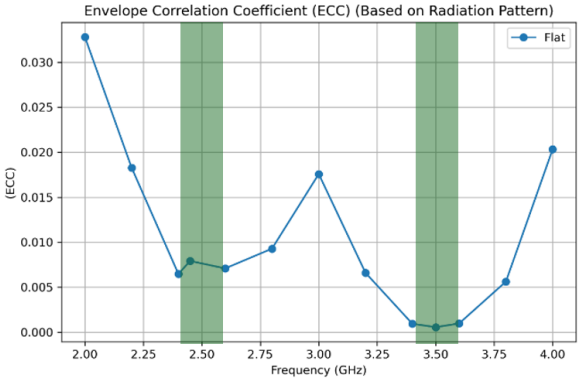

FIGURE 21. ECC for the proposed MTM MIMO antenna based on radiation pattern with polarization components.

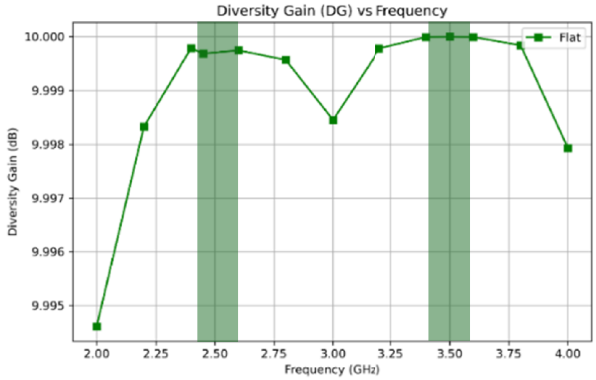

FIGURE 22. DG of the proposed MTM MIMO antenna.

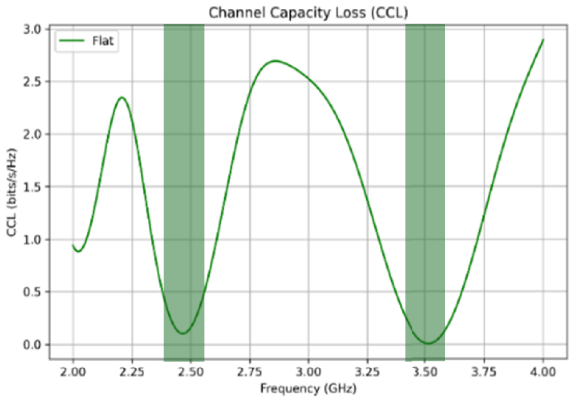

FIGURE 23. CCL of the proposed MTM MIMO antenna.

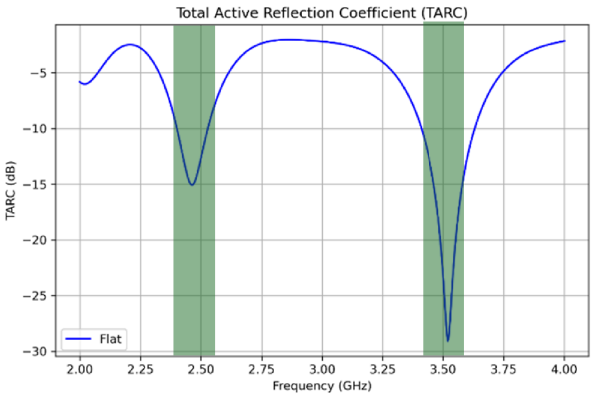

FIGURE 24. TARC of the proposed MTM MIMO antenna.

Channel Capacity Loss (CCL) is an important statistic for evaluating the performance of MIMO antenna systems because it measures the loss in system capacity caused by antenna element correlation. For an efficient MIMO system, the CCL should be as low as feasible, with values of less than 0.4 bits/s/Hz [19] commonly accepted. The CCL is computed and stated as follows:

$$CCL = -\log_2 det\,(R)$$

Here, R represents the correlation matrix that captures the interrelationship between the antenna ports, and *det* is the determinant of matrix R. The matrix is defined as:

$$R = \begin{bmatrix} \rho_{11} & \rho_{12} \\ \rho_{21} & \rho_{22} \end{bmatrix}$$

where ρ_{11} and ρ_{22} represent the self-correlation terms for Antenna 1 and Antenna 2, respectively. These terms account for the power reflection and coupling at each antenna port and are calculated as:

$$\rho_{ii} = 1 - \left(|S_{ii}|^2\right) - \left(|S_{ij}|^2\right)$$

ρ_{12} and ρ_{21} represent the mutual correlation terms between the two antenna ports and are calculated as:

$$\rho_{ij} = -\left(S_{ii}^* S_{ij} + S_{ij}^* S_{jj}\right)$$

Figure 23 depicts the CCL analysis of the proposed MTM MIMO antenna, demonstrating its performance across the 2 GHz to 4 GHz frequency range. Throughout the frequency range, the CCL varies but remains far below the essential threshold of 0.4 bits/s/Hz at the primary working frequencies (2.45 GHz and 3.5 GHz), demonstrating the antenna's efficacy in minimizing capacity loss. Fig. 24 demonstrates that the Total Active Reflection Coefficient (TARC) remains below -10 dB, indicating steady impedance behavior during multiport stimulation.

3.7. Surface Current Distribution

Figure 25 demonstrates the surface current distribution of the proposed MIMO antenna simulated using CST Microwave Studio. Figs. 25(a) and 25(b) show the current intensity for Port 1 and Port 2, respectively, and Fig. 25(c) indicates the current distribution for the MTM unit cell array. The differences in the surface current distribution for various frequencies are due to the changing currents on the surface of the antenna.

3.8. Free Space Measurement

The simulated and measured results in Fig. 26 illustrate a satisfactory agreement in resonance trends, validating the accuracy of the antenna design, although some minor frequency shifts and amplitude variations are evident. These changes are due to

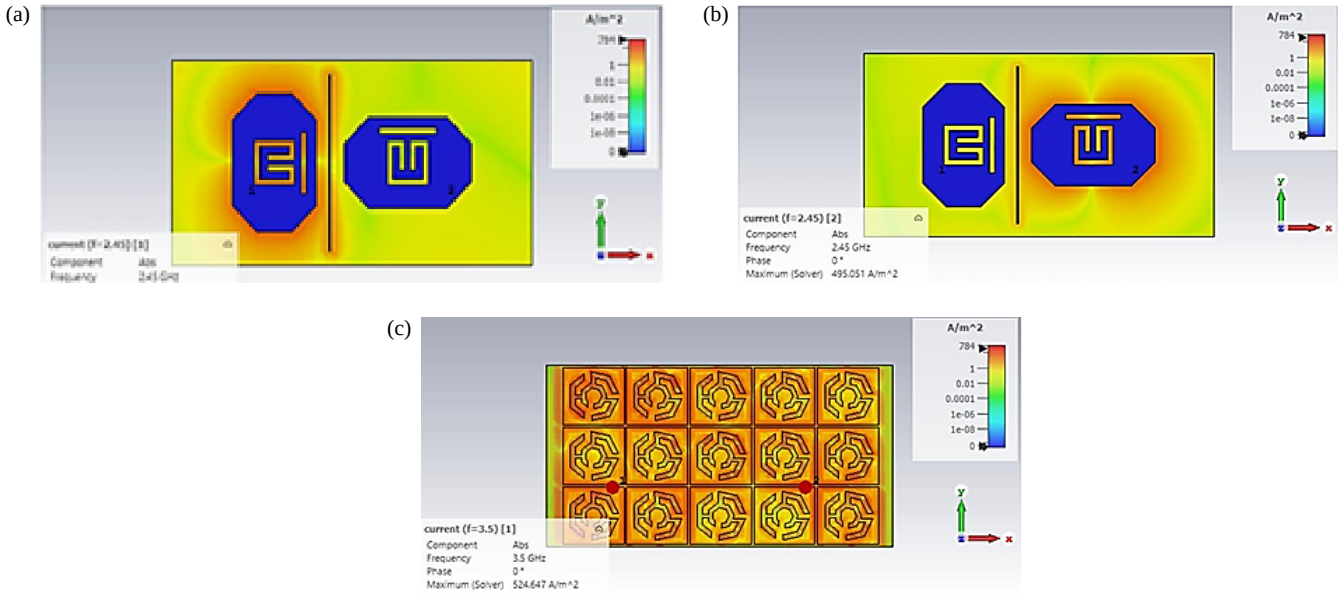

FIGURE 25. Surface current distribution at (a) Port 1, (b) Port 2, and (c) MTM unit cell array.

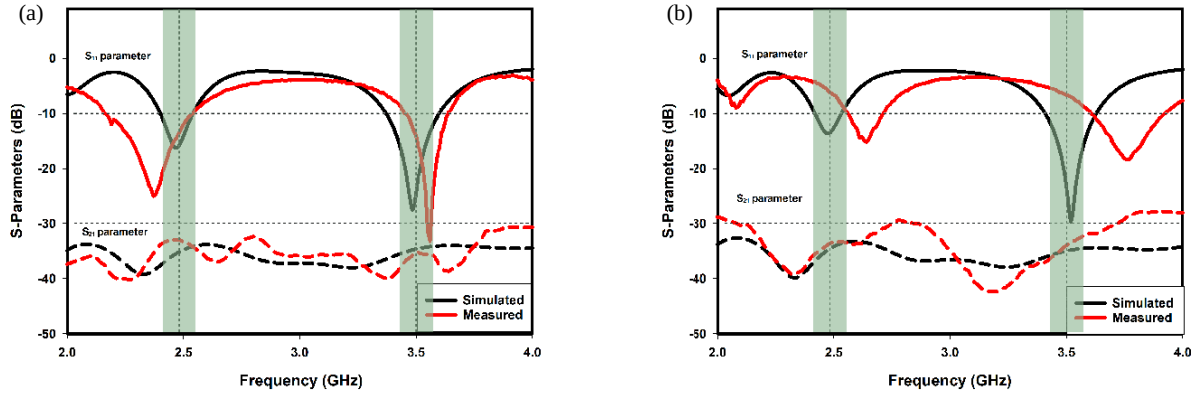

FIGURE 26. Simulated and measured S_{11} and S_{21} parameters of the proposed MIMO antenna (a) without and (b) with MTM unit cell array.

various factors related to the practical aspects of antenna fabrication and measurement, including inaccurate dimensions during cutting and stitching of the textile materials, soldering, and connector positioning; inaccurate thickness of the substrate materials during compression; and some minor imperfections in the measurement setup, including connector losses and calibration residuals.

3.9. RSSI Measurement

RSSI analysis is a quantitative method of assessing the strength of wireless signals received by an antenna or communication device. Usually measured in dBm units, RSSI is a signal quality indicator and is commonly used for assessing the performance of antennas, wireless modules, and communication systems in various conditions, such as distance, orientation, and environmental interference. RSSI analysis is also used to determine coverage areas and regions with signal degradation, thus facilitating antenna optimization and design improvements to improve wireless communication performance. This method is commonly employed in IoT, Wireless Fidelity (Wi-Fi), and other wireless communication systems [21]. From the results shown in Table 4, it is clear that RSSI values decrease with an increase in distance due to path loss. For distances of 1–2 m,

TABLE 4. RSSI measurement between ESP32 integrated with the proposed MIMO antenna and the mobile application.

P	D (m)	ESP32		
		Without Antenna	With Antenna	
			Port 1	Port 2
RSSI (dBm)	1	−58	−63	−61
	2	−68	−69	−62
	3	−70	−70	−65
	4	−73	−71	−68
	5	−78	−73	−70
	6	−82	−78	−72
	7	−84	−77	−75
	8	−88	−82	−79
	9	−91	−84	−83
	10	−94	−89	−85

TABLE 5. Vital signs parameters.

Parameter	Subject		
	1	2	3
SpO_2 (%)	98	100	97
Heart Rate (bpm)	60	75	68
Body Temperature	37	36	37

TABLE 6. Proposed design comparison with recent studies.

Ref.	Antenna Size (mm^2)	f (GHz)	Gain (dBi)	S_{11} (dB)	Isolation/S_{21} (dB)
[10]	80×80	3.08–7.75	8.3	< -10	≤ -15.5
[12]	110×106	2.45	5.8	< -10	≤ -40
[13]	44×44	5.6	7.95	< -10	≤ -19.85
[14]	60×44	5.0−6.6	9.5	< -10	< -34.8
[15]	37×44	4	3.28	< -10	14
[16]	55×44	4.9	8	< -10	-42.88
[17]	67.4×67.4	2.85	5	< -10	-15
Propose	133.2×70	2.45, 3.5	2.45 at 2.45 GHz 6.43 at 3.5 GHz	< -10	< -30

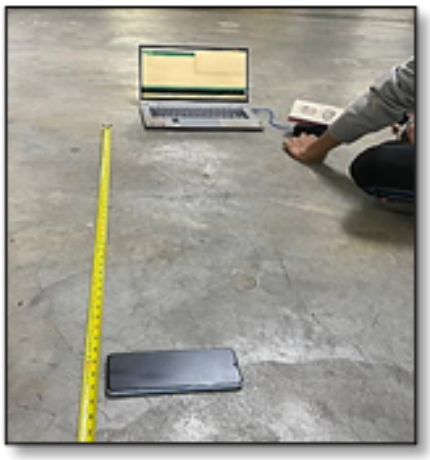

FIGURE 27. The distance between the hardware and mobile application is 1 m.

the ESP32 module without the proposed antenna has a higher RSSI value, as its internal antenna is adequate for short-distance communication. However, for distances between 3 m and 10 m, the ESP32 module with the proposed antenna has higher RSSI values, thus indicating the superiority of the proposed antenna over the internal antenna at the same distance. Fig. 27 shows the experimental setup with a 1 m distance between the hardware and mobile application (MIT App Inventor). Table 5 shows the readings of SpO_2, heart rate, and body temperature taken from three subjects, which validate the integration of the MAX30102 and LM35 biomedical sensors with the designed antenna for RHMS. Overall, the proposed antenna exhibits higher and more stable RSSI values, indicating stronger and more reliable signal reception. This indicates that the suggested antenna delivers better gain and decreases signal deterioration over distance, thereby enhancing communication reliability [21]. Table 6 compares the proposed dual-band MIMO antenna with recent designs, showing that it offers a dual-band operation, high gain of 6.43 dBi, and good MC (< -30 dB), making it suitable for wearable biomedical sensing applications.

4. CONCLUSION

The suggested dual-band textile C-shaped CSR MIMO antenna has been successfully developed and measured at 2.45 GHz and 3.5 GHz. The suggested MIMO antenna improved the realized gain on both ports. At 2.45 GHz, the simulated realized gain is 2.45 dBi. The antenna also improved the simulated realized gain at 3.5 GHz, achieving 6.43 dBi. The simulated radiation efficiency at 3.5 GHz is 52% at Port 1 and 51% at Port 2. Besides, RSSI is improved when using the proposed antenna compared to that without the proposed antenna. This improvement in RSSI is particularly beneficial for the transmission of vital sign data from hardware using the MIT App Inventor mobile application. A stronger signal ensures reliable data transfer, reducing data loss or corruption.

ACKNOWLEDGEMENT

The authors would like to thank Universiti Malaysia Perlis [Grant Number: 9001-00752] and Songkhla Rajabhat University for financial assistance under the INTERES grant with Keysight (KS) Co. Ltd. [Grant Number: 9008-00042]. KS Co. Ltd. promotes expertise of testing and measuring for emerging technologies.

REFERENCES

[1] Musa, U., A. Smida, M. S. Yahya, M. I. Waly, J. J. Tiang, N. K. Mallat, S. Muhammad, and A. Salisu, "Machine learning-optimized dual-band wearable antenna for real-time remote pa-

tient monitoring in biomedical IoT systems," *Scientific Reports*, Vol. 15, No. 1, 30943, 2025.

[2] Lv, X., S. Rani, S. Manimurugan, A. Slowik, and Y. Feng, "Quantum-inspired sensitive data measurement and secure transmission in 5G-enabled healthcare systems," *Tsinghua Science and Technology*, Vol. 30, No. 1, 456–478, 2025.

[3] Salleh, S. M., M. F. Ain, Z. Ahmad, I. S. Z. Abidin, L. Y. Seng, and M. N. Osman, "Stretchable and bendable polydimethylsiloxane-silver composite antenna on PDMS/air gap substrate for 5G wearable applications," *IEEE Access*, Vol. 11, 133 623–133 639, 2023.

[4] Li, M.-Y., Y.-L. Ban, Z.-Q. Xu, J. Guo, and Z.-F. Yu, "Tri-polarized 12-antenna MIMO array for future 5G smartphone applications," *IEEE Access*, Vol. 6, 6160–6170, 2018.

[5] Ahmad, J. and M. Hashmi, "Reduced inter-element interference mmWave MIMO antenna and its application in WBAN," *IEEE Access*, Vol. 13, 70 947–70 963, 2025.

[6] Mashagba, H. A., H. A. Rahim, I. Adam, M. H. Jamaluddin, M. N. M. Yasin, M. Jusoh, T. Sabapathy, M. Abdulmalek, A. A. Al-Hadi, A. M. Ismail, and P. J. Soh, "A hybrid mutual coupling reduction technique in a dual-band MIMO textile antenna for WBAN and 5G applications," *IEEE Access*, Vol. 9, 150 768–150 780, 2021.

[7] Wang, J., C. Du, J. Chu, and R. Li, "A wearable CPW-fed quad-band-notched two-port MIMO antenna for IoT applications," *Progress In Electromagnetics Research C*, Vol. 164, 243–252, 2026.

[8] Gali, R. L. and M. Tatineni, "Optimized NCP MIMO antenna with dual diamond slots for enhanced isolation in 5G applications," *Progress In Electromagnetics Research C*, Vol. 165, 25–34, 2026.

[9] Kumkhet, B., P. Rakluea, N. Wongsin, P. Sangmahamad, W. Thaiwirot, C. Mahatthanajatuphat, and N. Chudpooti, "SAR reduction using dual band EBG method based on MIMO wearable antenna for WBAN applications," *AEU — International Journal of Electronics and Communications*, Vol. 160, 154525, 2023.

[10] Hasan, M. M., M. T. Islam, M. Samsuzzaman, M. H. Baharuddin, M. S. Soliman, A. Alzamil, I. I. M. A. Sulayman, and M. S. Islam, "Gain and isolation enhancement of a wideband MIMO antenna using metasurface for 5G sub-6 GHz communication systems," *Scientific Reports*, Vol. 12, No. 1, 9433, 2022.

[11] Govindan, T., S. K. Palaniswamy, M. Kanagasabai, S. Kumar, M. Marey, and H. Mostafa, "Design and analysis of a flexible smart apparel MIMO antenna for bio-healthcare applications," *Micromachines*, Vol. 13, No. 11, 1919, 2022.

[12] Shamsuri Agus, A. N. S., T. Sabapathy, M. Jusoh, M. A. Abdelghany, K. Hossain, S. Padmanathan, S. S. Al-Bawri, and P. J. Soh, "Combined RIS and EBG surfaces inspired meta-wearable textile MIMO antenna using viscose-wool felt," *Polymers*, Vol. 14, No. 10, 1989, 2022.

[13] Wu, R., J. Dong, and M. Wang, "Wearable polarization conversion metasurface MIMO antenna for biomedical applications in 5 GHz WBAN," *Biosensors*, Vol. 13, No. 1, 73, 2023.

[14] Althuwayb, A. A., M. Alibakhshikenari, B. S. Virdee, N. Rashid, K. Kaaniche, A. B. Atitallah, A. Armghan, O. I. Elhamrawy, C. H. See, and F. Falcone, "Metasurface-inspired flexible wearable MIMO antenna array for wireless body area network applications and biomedical telemetry devices," *IEEE Access*, Vol. 11, 1039–1056, 2023.

[15] Mood, Y. and R. Pandeeswari, "Complementary folded line metamaterial loaded MIMO antenna for S-band applications," *Progress In Electromagnetics Research C*, Vol. 150, 145–155, 2024.

[16] Song, Z., S. Zhao, S. Li, J. Chen, and Y. Xue, "High-isolation compact MIMO antenna with distributed metamaterial loading," *Progress In Electromagnetics Research M*, Vol. 128, 51–59, 2024.

[17] Jaouad, S., C. Chahboun, M. A. Ennasar, O. E. Mrabet, J. R. P. Lopez, M. Khalladi, and M. Aznabet, "Metasurface-driven improvement in MIMO antenna performance by addressing mutual coupling," *Progress In Electromagnetics Research C*, Vol. 163, 73–80, 2026.

[18] Hussain, A., J. Dong, Y. I. Abdulkarim, R. Wu, F. F. Muhammadsharif, R. Shi, and M. M. R. Howlader, "A double negative (DNG) metamaterial based on parallel double-E square split resonators for multi-band applications: Simulation and experiment," *Results in Physics*, Vol. 46, 106302, 2023.

[19] Yang, S., L. Liang, Z. Li, and W. Wang, "Ultrawideband MIMO circularly polarized cube antenna with characteristic mode analysis for wireless communication and sensing," *IEEE Internet of Things Journal*, Vol. 11, No. 7, 12 192–12 202, 2024.

[20] Jemaludin, N. H., A. J. A. Al-Gburi, R. H. Elabd, T. Saeidi, M. F. Akbar, I. M. Ibrahim, and Z. Zakaria, "A comprehensive review on MIMO antennas for 5G smartphones: Mutual coupling techniques, comparative studies, SAR analysis, and future directions," *Results in Engineering*, Vol. 23, 102712, 2024.

[21] Ali, W., Nizam-Uddin, M. Zahid, and S. Shoaib, "Performance analysis and design optimization of wearable RFID sensor-antenna system for healthcare applications," *IEEE Access*, Vol. 13, 145 540–145 555, 2025.